UC Berkeley
UC Berkeley Previously Published Works

Title

Detecting onset of lithium plating during fast charging of Li-ion batteries using operando electrochemical impedance spectroscopy

Permalink

https://escholarship.org/uc/item/9q16g8z9

Journal

Cell Reports Physical Science, 2(10)

ISSN

2666-3864

Authors

Brown, David E
McShane, Eric J
Konz, Zachary M
et al.

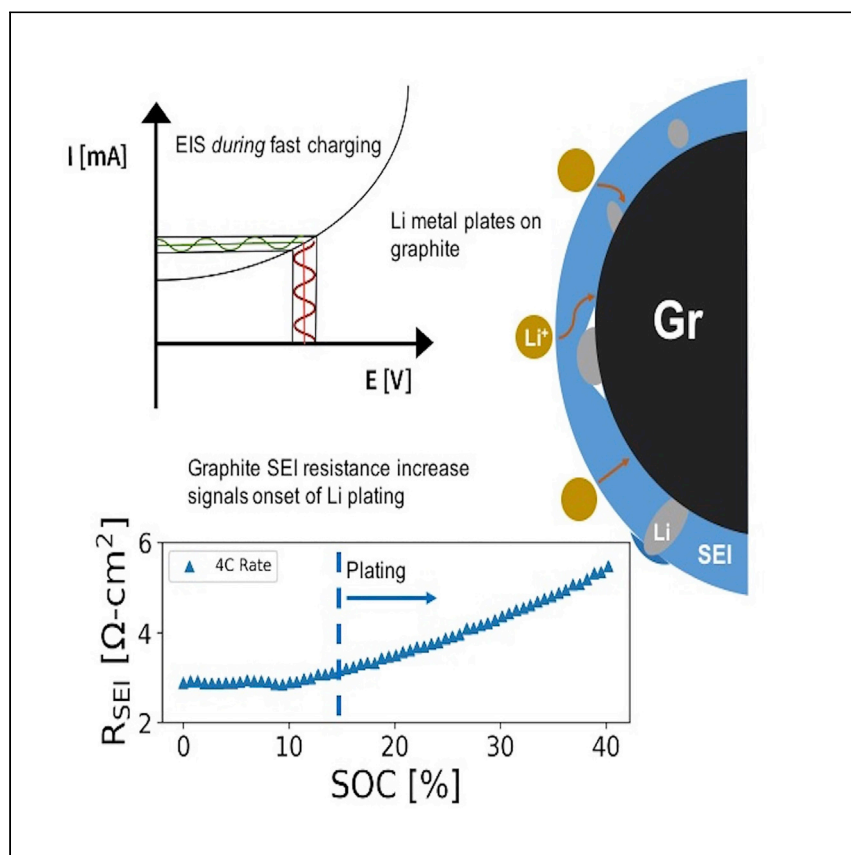**Publication Date**

2021-10-01

DOI

10.1016/j.xcrp.2021.100589

Copyright Information

Peer reviewed

Article

Detecting onset of lithium plating during fast charging of Li-ion batteries using operando electrochemical impedance spectroscopy

Electric vehicle Li-ion battery charging times are slow to prevent lithium plating, a detriment to cycle life and safety, on the graphite electrode. Brown et al. detect the onset of lithium plating during fast charging using electrochemical impedance spectroscopy. With further development, this technique could enable fast charging in existing charging infrastructure.

David E. Brown, Eric J. McShane, Zachary M. Konz, Kristian B. Knudsen, Bryan D. McCloskey

bmcclosk@berkeley.edu

Highlights

Li plating onset detected on graphite anode using electrochemical impedance spectroscopy

High Li detection sensitivity (<0.6% graphite capacity) during high charge rates (4C)

Plating detection cross-validated with *ex situ* mass spectrometry Li metal titrations

Impedance feasibility demonstrated in commercially relevant two-electrode cells

Article

Detecting onset of lithium plating during fast charging of Li-ion batteries using operando electrochemical impedance spectroscopy

David E. Brown,[1,2] Eric J. McShane,[1,2] Zachary M. Konz,[1,2] Kristian B. Knudsen,[1,2,3] and Bryan D. McCloskey[1,2,4,*]

SUMMARY

Electrochemical plating of Li metal on the graphite electrode is the key limitation behind slow charging times of Li-ion batteries (LIBs) in electric vehicles (EVs). Currently, electrochemical methods to detect the onset of Li plating while a battery is fast charging are sparse. In this study, we use *operando* electrochemical impedance spectroscopy to reliably detect the onset of Li plating on graphite electrodes in three-electrode LIBs. An increase in the graphite solid-electrolyte interface (SEI) resistance indicates that Li plating has occurred. By cross-validating with a highly sensitive *ex situ* chemical titration, we determine that this technique can detect very small amounts of plated Li (<0.6% of the graphite electrode's capacity). We also offer physical explanations for the observed impedance behavior. Finally, we show that this technique can be applied to standard two-electrode LIB systems, making the method an important step toward safely implementing fast charging protocols for LIBs in EVs.

INTRODUCTION

Li-ion batteries are the industry standard for energy storage in devices in applications ranging from personal electronics to electric vehicles (EVs). To help broaden the adoption and use of EVs, substantial research has focused on enabling "extreme fast charging" (XFC),[1] where charging times would be comparable to the time it takes to fill a fuel tank. For example, the US Department of Energy has set a goal to achieve a 200-mile charge in 10 min.[2]

However, understanding, and ultimately eliminating, unwanted Li plating on the graphite anode currently prevents commercial adoption of XFC protocols.[1,3,4] During charge, the lithium transition metal oxide cathode is oxidized, releasing Li^+ ions into the electrolyte. The Li^+ then transports through the non-aqueous electrolyte to the graphite anode. Once there, it is reduced and, ideally, intercalates between the graphene sheets of the graphite. The thermodynamic equilibrium potential window within which LiC_6 (lithiated graphite) forms is in the range of approximately 1–100 mV versus Li/Li^+, just slightly above the potential at which Li metal formation can occur (Li metal formation is favorable below 0 V versus Li/Li^+).[3] To drive high graphite lithiation rates, the requisite reduction overpotentials are sufficiently large to drop the graphite operating potential below 0 V versus Li/Li^+, and hence, plating becomes thermodynamically possible. Beyond the kinetic surface overpotential, additional voltage drops due to Li^+ concentration gradients and ohmic losses in the electrolyte scale with applied current and can be sizable at high rates.[3,5]

[1]Department of Chemical and Biomolecular Engineering, University of California, Berkeley, Berkeley, CA 94720, USA

[2]Energy Storage and Distributed Resources Division, Lawrence Berkeley National Laboratory, Berkeley, CA 94720, USA

[3]Present address: Unisense A/S, Aarhus 8200, Denmark

[4]Lead contact

*Correspondence: bmcclosk@berkeley.edu

https://doi.org/10.1016/j.xcrp.2021.100589

Li plating can cause dangerous failure of the battery or, at a minimum, the loss of capacity over the lifetime of the battery. If enough Li plates, dendrites form on the graphite surface. If these dendrites puncture the separator and make contact with the cathode, the battery will short. This can release a tremendous amount of heat, possibly igniting the flammable non-aqueous electrolyte, posing a serious safety concern for XFC. Even if dendrites do not form, the plated Li can become electronically isolated from the electrode through parasitic processes. Once this occurs, the capacity of the battery has necessarily decreased.[6,7] Plated Li can become delaminated from the graphite surface, lodged in the solid electrolyte interphase (SEI) layer on the graphite, or detached from a larger Li deposit that has partially chemically intercalated into the graphite. This Li may also react with electrolyte, promoting further battery degradation and reduced electrolyte performance.[8]

Currently, there is no electrochemical method to reliably, and precisely, detect the onset of Li plating during XFC, i.e., while the battery is charging.[4,9] A few methods can detect Li plating after XFC. If Li metal is present, a stripping plateau can be observed in the discharge voltage profile of the graphite upon immediate discharge of the battery (often referred to as the dQ/dV method). This plateau can be used to detect plated Li if it has occurred, although it requires an appreciable amount of Li to be present on the surface.[10] Our prior work has shown that differential voltage analysis of cell potentials at rest after XFC can reliably detect Li plating, but it necessarily requires analysis after charging during a 30-min rest period.[7] To quantify Li plating, we have also developed a *post mortem* mass spectrometry titration technique to correlate hydrogen gas evolved by the reaction of the species deposited on the graphite with acid to the amount of plated Li and carbon dioxide produced to the amount of SEI on the surface.[8] Li is also often visually observed upon *post mortem* analysis of fast charged graphite electrodes.[5,11] Although monitoring the potential of graphite is theoretically a viable way to detect plating,[5,12] it is not consistently reliable. A potentiostat or battery management system will measure the average potential of all the graphite particles with which it is in contact. Particles closer to the separator will likely drop to a plating-favorable potential before those closest to the current collector. This means that plating may be occurring before a total measured potential change would indicate. Given the similar potentials of lithiated graphite and metallic Li, as well as the similar chemical nature of the two species, no technique to date has been able to detect the onset of Li plating on graphite *during* fast charging, as discussed more completely elsewhere.[4,9] This includes traditional impedance analysis, where changes in Nyquist or Bode plots have only been reported during open circuit rest of the battery and not during charge,[13–15] or the cell resistance is otherwise calculated during brief pauses in cell charging.[16]

Instead, we propose to combine operando electrochemical impedance spectroscopy (EIS), where impedance measurements are collected during fast charging, with a method of impedance analysis called the distribution of relaxation times (DRT), which shows improved process deconvolution over traditional equivalent circuit analysis of Nyquist or Bode plots. DRT is able to deconvolute signals based on the time constants, τ = the resistance multiplied by the capacitance, of individual processes in the electrochemical system. For example, Figure 1 compares the Nyquist (Figure 1A), imaginary impedance versus frequency (Figure 1B), and DRT (Figure 1C) representations of a single operando impedance scan on a graphite electrode undergoing a modest rate (2C) charge. For interfacial processes that behave as parallel resistor-capacitor (RC) or resistor-constant phase element (RQ) circuit elements with sufficiently different time constants, each process should show a peak in the imaginary impedance versus frequency representation. In Figure 1B, however, there is only one clear maximum, although the DRT in Figure 1C more
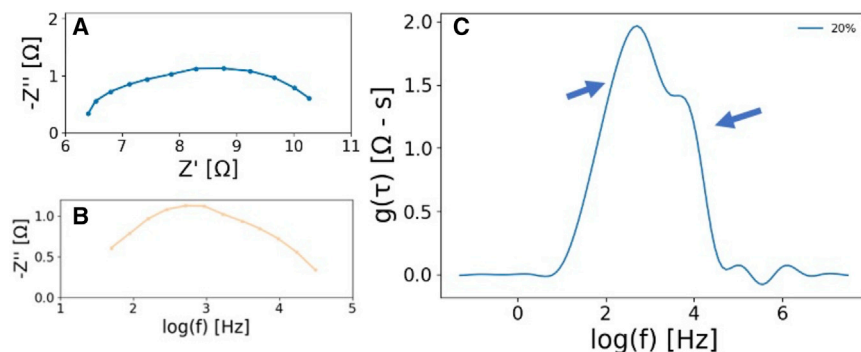
Figure 1. Comparison of traditional impedance analyses to DRT

High-frequency (100 kHz–50 Hz) impedance gathered during a 2C charge of a graphite electrode in a three-electrode cell.

(A) The Nyquist representation of the data, which shows one broad semi-circle.

(B) The imaginary impedance plotted versus the frequency of the data, which shows one broad peak. RC/RQ-type processes show peaks in this representation.

(C) The DRT transform of the impedance data, which shows two clear peaks over the frequency range measured. This indicates the presence of two physical processes that have similar time constants.

clearly indicates two peaks, meaning that there are two processes here with very similar time constants. Without previous knowledge of the system, one may attempt to fit these data many different ways, with various numbers of in-series RC circuit elements. DRT allows us to develop more physically accurate model analyses for graphite electrodes during fast charging.

The DRT has been used to evaluate the performance of solid oxide fuel cells,[17] as well as to deconvolute processes on graphite electrodes[15,18–21] and for overcharged LIB full cells.[14] The time transformation of the transmission line impedance model, a similar mathematical procedure to the DRT, has also been previously developed to predict Li plating during relaxation after charging.[22] Katzer and Danzer have also used DRT to detect Li plating by monitoring the relaxation of the impedance after charging. They show a very high sensitivity to Li plating, but it does require at least a 15-min rest period after charging to accurately detect Li deposition.[15]

DRT analysis of EIS data is used here to detect the onset of Li plating during fast charge, where the response of the system to the presence of plated Li can be resolved. This is cross-validated with mass spectroscopy titration (MST) techniques,[8] and it is found to have a high sensitivity to Li plating on graphite (<0.6% of graphite capacity). Furthermore, we demonstrate the applicability of this technique to more commercially relevant two-electrode full cells.

RESULTS AND DISCUSSION
Graphite impedance response to Li plating

To first determine whether there is any DRT response related to plating, we gathered potentiostatic impedance 30 min into open-circuit voltage (OCV) relaxation (100 kHz to 50 mHz; 0 V versus OCV; 5 mV amplitude) after charging a battery to different states-of-charge (SOCs) at a low rate (C/5), including to SOCs above the full lithiation of graphite to intentionally force Li plating on the graphite surface. We have confirmed that no Li plating occurs during a C/5 charge prior to the full lithiation (370 mAh/g) of the graphite.[8] Figure 2A shows the DRT analysis of the impedance spectra gathered after each SOC shown. The peak just below 10^4 Hz is related to Li^+ ion movement through the SEI.
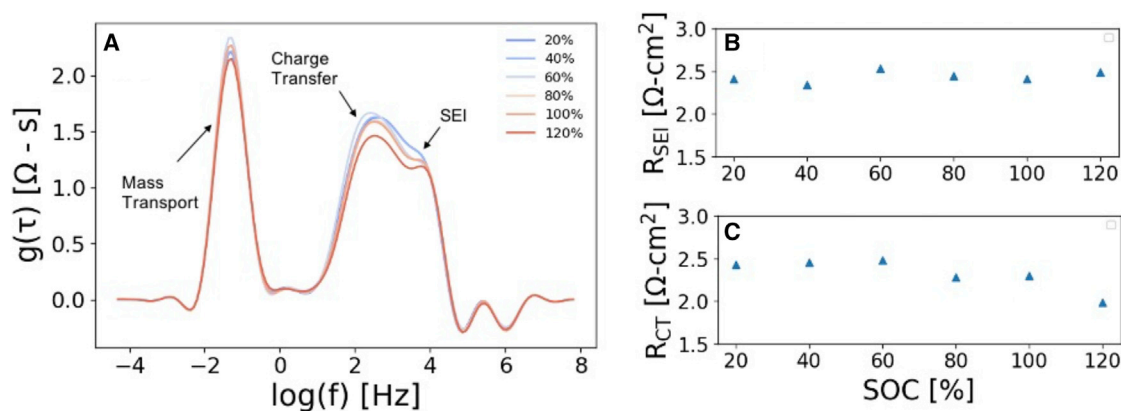
Figure 2. Graphite response to lithiation and plating after C/5 charges

(A) DRT spectra from potentiostatic impedance measurements of graphite at OCV after being charged at a C/5 rate to different SOCs in a graphite/NMC532/AuLi three-electrode cell. Each line represents a different SOC, where "100%" is the capacity where all of the graphite is expected to be lithiated (370 mAh/g).

(B) The resistance values from fitting an RQ circuit to each 10^4 Hz peak, corresponding to Li^+ movement through the SEI.

(C) The resistance values from fitting an RQ circuit to each peak at approximately 10^2 Hz, corresponding to the charge transfer process at the graphite surface.

See also Note S2 for peak assignment information.

The peak near 10^2 Hz is attributed to the charge transfer resistance of the lithium redox reaction (i.e., either Li^+ insertion or Li plating). The peak at 10^{-1} Hz contains information about the mass transport of Li^+ ions throughout the system. This peak will be dominated by the diffusion process with the lowest characteristic time. In a standard cell with a single Celgard separator, this is typically the solid-state diffusion of Li in the graphite,[18] but given the number of separators used for this three-electrode cell, the bulk electrolyte diffusion is a non-negligible contributor to the mass transport impedance. Although the presence of electrochemically active metallic Li could affect diffusive processes throughout the cell, the peak at 10^{-1} Hz does not show a discernible trend upon plating. This varies with SOCs, because the method of solving the DRT used herein cannot adequately resolve diffusive and capacitive processes. This information can be more accurately captured using the distribution function of differential capacity,[23] although this is not necessary for this analysis, given that Li plating clearly affects the higher frequency interfacial processes. The reasoning for this process assignment is explained in greater detail in Note S2.

By examining the spectra in Figure 2A, we see that the SEI and charge transfer processes are approximately constant until full lithiation of the graphite (i.e., 100% SOC). However, upon over-lithiation of the graphite, there is a clear depression in the peak height of both processes. For quantitative comparison, each peak is fit with an RQ circuit to precisely extract the resistances and capacitances of each process. The fitting process is explained in more detail in Figure S4. The resistance values from these fits are shown in Figures 2B and 2C. These data confirm that the resistances of both SEI transport and the charge transfer process are approximately constant prior to over-lithiation. Upon over-lithiation (120% SOC), the resistance of the SEI (Figure 2B) stays constant. This suggests that low-rate Li plating above 100% SOC occurs at the graphite/SEI interface, rather than the SEI/separator interface, and additional SEI species are not formed (i.e., the SEI thickness does not change). The charge transfer resistance (Figure 2C), however, decreases upon over-lithiation of the graphite. This is reasonable, given that Li stripping and plating likely has comparatively fast kinetics to the graphite insertion/deinsertion process, as
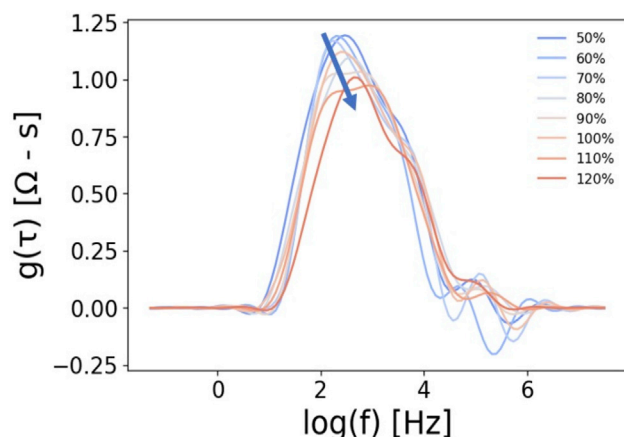
Figure 3. Graphite response during C/5 over-lithiation
DRT spectra analyzed at different SOCs from galvanostatic impedance measurements of graphite over-lithiated at a C/5 charge rate with an AC amplitude equal to 50% of that rate.

discussed by Chen et al.,[14] who studied the DRT response of over-lithiated full cells and also see a charge transfer resistance decrease upon over-lithiation.

Given the data in Figure 2, it is clear that there is an impedance response to Li plating at frequencies above 10 Hz. Therefore, we reduce the frequency range of subsequent EIS measurements, from 100 kHz–50 mHz to 100 kHz–50 Hz, to significantly reduce the measurement time for each EIS scan (from 1.5 min/scan to ~6 s/scan, respectively). This enables the collection of quality impedance data, as confirmed by Kramers-Kronig (KK) analysis (see Figure S1 and supplemental experimental procedures), during high-rate charging.

Figure 3 shows a similar charge transfer resistance drop during galvanostatic (active lithiation) impedance analysis, in which intentional over-lithiation is again performed (C/5 DC current, amplitude 50% of DC). These data qualitatively have a higher level of noise, because graphite has very stable potential plateaus during phase transformations.[24] This means that the applied alternating current at a low rate of DC charge will lead to a small potential response, effectively creating a lower signal-to-noise ratio than the alternating potential applied for the experiment above (see Figure S2 and Note S1). However, the same general trend is observed, and importantly, Figure 3 indicates that impedance data can be reliably gathered during charge.

For the purposes of Li plating detection during XFC, however, it is crucial to extract quantitative resistance values from the DRT analysis for data obtained at higher rates. Figure 4 presents the resistance extracted at the charge transfer peak and the SEI peak normalized to their values immediately upon applying a charging current for three different charging current rates. Figure 4 demonstrates that we can, indeed, quantify the *operando* resistance changes of the graphite for rates at least up to 6C. The higher rate impedance data have notably different behavior from that of the C/5 charging data. C/5 charging shows relatively constant SEI and charge transfer impedance up to 100% SOC, followed by a charge transfer impedance decrease upon plating due to over-lithiation above 100% nominal SOC (Figure 2). However, Figure 4 clearly shows an increase in the impedance of both the charge transfer process and the SEI at a SOC well below 100%. This relative change from the initial resistance values is clearly observed for both the 4C and 6C rates, though
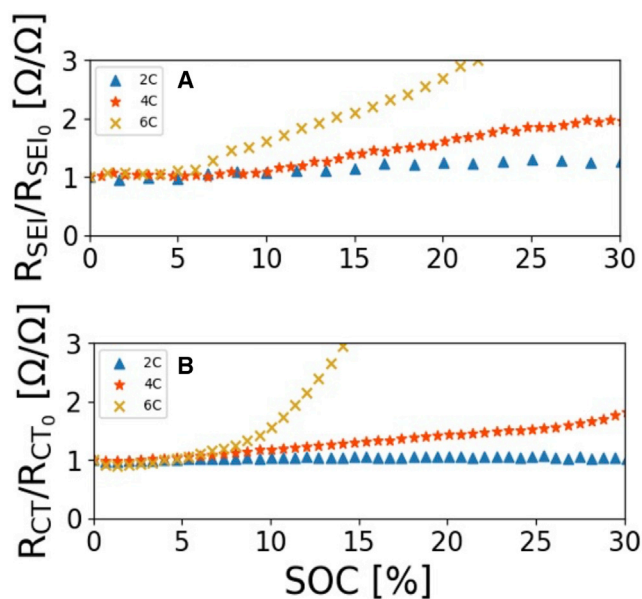
Figure 4. Graphite resistances extracted during different rates of fast charging
(A) Fitted graphite SEI resistances from single charges at 2C, 4C, and 6C.
(B) Fitted graphite charge transfer resistances from single charges at 2C, 4C, and 6C. All values are normalized to the resistance values fitted at 0% SOC, which are denoted as R_{SEI0} and R_{CT0}.

the former has lower relative increases in each case. Comparing the SEI and charge transfer resistance increases at the different rates, there is a slightly earlier SOC onset for the SEI impedance rise with increasing rate. Furthermore, although a rise in the SEI resistance is easily observed in the 4C charge, changes to the 4C charge transfer resistance are slightly less clear, although also increasing throughout the charge.

To further explore this impedance response during XFC, different cells were cycled multiple times at 4C to different SOCs. 4C was chosen for this study because it provides a larger SOC window before plating compared to the early SOC plating expected for 6C. Figure 5 details the results of collecting impedance during the charge steps of cycled $LiNi_{0.5}Mn_{0.3}Co_{0.2}O_2$ (NMC532)/Gr/AuLi three-electrode cells. The cells are charged at 4C to 10% SOC, allowed to relax for 30 min, and then discharged at a rate of C/2. This cycling (with charge to 10% SOC) is repeated two additional times. This same procedure is then repeated for three cycles to 20% SOC (with similar relaxation time and C/2 discharge), then 30% SOC, and finally 40% SOC.

Figure 5 presents the fitted impedance values during one of the three cycles to 20%, 30%, and 40% SOC. Figure 5A indicates that a significant SEI impedance rise appears to commence around 15%–20% SOC. If this impedance response indicates Li plating, this is presumably the SOC where the onset of Li plating occurs. There is also a very slight increase in R_{SEI} from 0% to 15%, which could be due to small amounts of Li plating and/or SEI formation from electrolyte reduction during the fast-charging process.

Figure 5B indicates that the charge transfer resistance also increases with increasing SOC, with a consistent cycle-to-cycle onset of the increase at approximately 5% SOC. This is notably earlier than the 20% SOC onset of the SEI impedance rise seen in Figure 5A. The charge transfer resistance is a function of many variables,
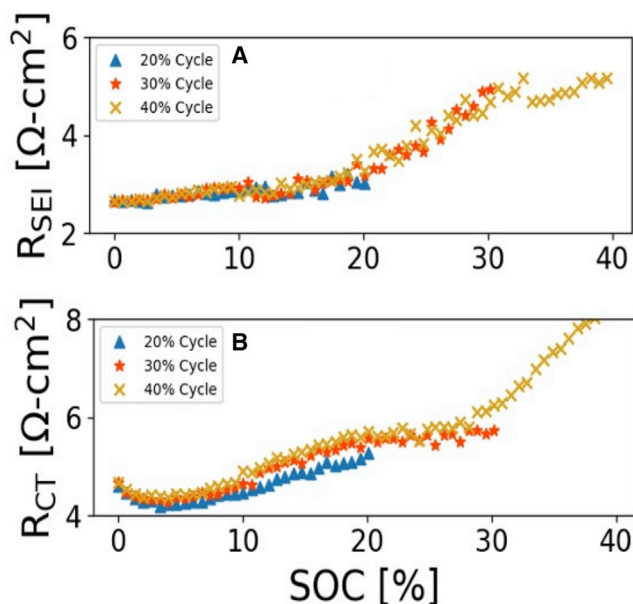
Figure 5. Graphite resistances during 4C charging to different SOCs
Fitted R_{SEI} (A) and R_{CT} (B) for graphite charged for the third of three charges at 4C to 20%, 30%, and 40% SOC, respectively, and discharged at C/2.

including the surface concentration of the reactant species, i.e., Li$^+$ at the graphite surface.[25] Li$^+$ concentration gradients will build over time as the battery is charged at high rates,[26] so an increase in the charge transfer resistance is not unexpected nor does it necessarily indicate that Li plating has occurred. The charge transfer resistance increase consistently occurs before the SEI resistance increase, so we cannot rule out the possibility that it could provide either a more sensitive Li plating detection signal than the SEI resistance or a method to predict when Li plating will occur. To determine which of these impedance responses, if either, is related to Li plating, additional cross-validation experiments were performed.

To better understand the physical origin of the impedance behavior observed and to link it to Li plating, we employ the acid titration technique outlined by McShane et al.,[8] which is detailed in the Experimental Procedures section. Graphite electrodes were cycled following the same procedure described for Figure 5. After the final cycle, the graphite was deep discharged to 1.5 V versus Li/ Li$^+$ and then extracted, rinsed with dimethyl carbonate (DMC), and titrated using mass spectrometry titrations (MSTs). This technique has been previously developed in our lab to quantify surface species on Li-ion battery cathodes, as well as to detect the presence of "inactive Li" in graphite electrodes. It takes advantage of the reaction of lithium metal with water to form hydrogen gas that can be precisely measured by a mass spectrometer, with a resolution down to ~10 nmol (~0.3 μAh) inactive Li. Although this technique cannot distinguish between lithiated graphite and electronically isolated, plated Li metal, it still provides a very sensitive way to measure Li inventory lost due to XFC.[8]

The results of the titration data for this work are shown in Figure 6. In the cases of 0% SOC (i.e., formation cycling and deep discharge only), we do not expect any Li plating. The inactive Li measured here can simply be attributed to some electronically inaccessible lithiated graphite that forms during formation cycling. As shown
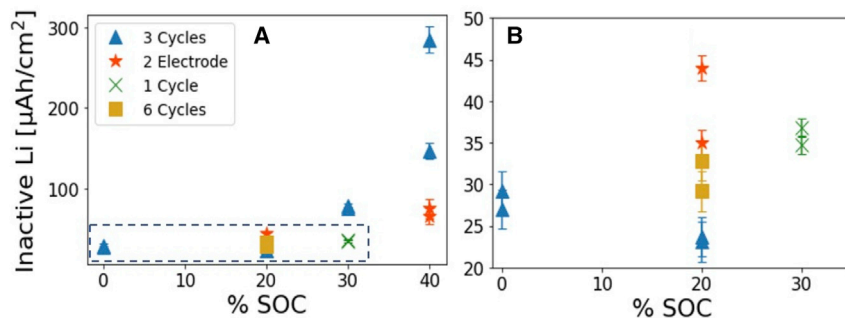
Figure 6. Inactive Li from MST of graphite after charging

(A) Measured inactive Li from MST of extracted and rinsed graphite electrodes post-cycling at a charge rate of 4C and deep discharge rate of C/2 to a graphite potential of 1.5 V versus Li/Li$^+$. The blue triangles are the results of electrodes cycled three times to the indicated SOC. The green crosses represent cells following the same cycling procedure, except only one charge at the final denoted % SOC. The red stars represent the inactive Li on a graphite electrode cycled in a standard two-electrode configuration of a NMC532/Gr. The yellow squares are the results of electrodes cycled six times to 20% SOC. 0% SOC denotes a graphite electrode that was only formed (see Cell assembly in Experimental procedures section), but not fast charged.

(B) Expanded view of data from (A) in the dotted box. The error bars are experimental error determined to be 10% of the measured value.

in Figure 5A, cycling to 20% SOC three times shows only a minor increase in the SEI resistance, although the charge transfer resistance has increased ~25% over its minimum value (Figure 5B). The titration results for two graphite electrodes charged under the same conditions indicate, within error, no increase in the inactive Li on the electrode surface relative to the 0% SOC electrode cases. This suggests no Li plating has occurred for these conditions or any Li plating that did occur was fully stripped during the deep discharge. This also suggests that, at least for the sensitivity limits and deep discharge requirements of the titration method, an increase in the charge transfer resistance is not an indicator of Li plating, whereas a significant increase in the SEI resistance may still be a viable Li plating indicator. The average value from these four cells (26 µAh/cm^2), the two 0% SOC electrodes and the two 20% SOC electrodes, represents the baseline of lost Li inventory and is consistent with our prior studies on similar electrodes.[8]

After cycling to 30% SOC three times, the impedance analysis shows a noticeable increase in the SEI resistance as the charge progresses above 20% SOC (Figure 5A), possibly indicating plating. Indeed, the titrations indicate an average 61 µAh/cm^2 rise in the amount of inactive Li above the 0% SOC baseline. Assuming that all of the additional H$_2$ is from plated Li and Li metal can be stripped with an efficiency of 70% (all titrations are performed on discharged electrodes),[7,8] the lithium titrated represents 2.7% of the graphite's capacity. However, we must account for the fact that these are measurements for the total amount of Li plated during three cycles of XFC. The per cycle amount of Li plating is much lower. And indeed, titrating graphite electrodes with the same three cycles to 10% and 20% but only a single 4C charge to 30% SOC shows a much lower amount of inactive Li: average 14 µAh/cm^2 above baseline, 0.6% graphite capacity (denoted as the green crosses in Figure 6). When combined, these results suggest that measuring the SEI resistance during fast charging is a reliable and sensitive indicator of Li plating.

As noted previously, for cells cycled three times to 20% SOC, there is a small increase in the SEI impedance compared to the initial SEI impedance, as seen in Figure 5A.
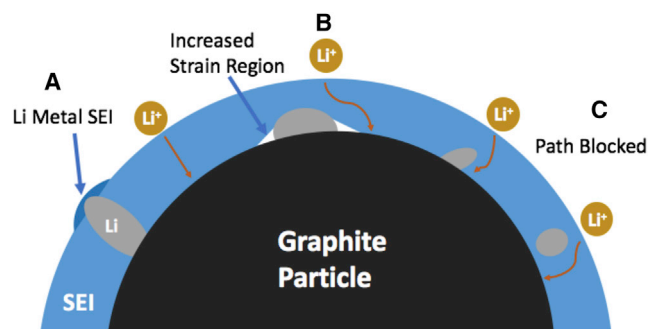
Figure 7. Possible mechanisms for the origin of the SEI impedance rise seen during XFC
(A) Li metal could react with the electrolyte to form additional SEI.
(B) Li metal deposits could protrude into the SEI, causing partial delamination of the SEI/increased contact resistance between the SEI and the graphite.
(C) Li metal deposits may obstruct Li^+ movement through the SEI.

However, titrations of electrodes cycled three times to 20% SOC show inactive Li amounts that are within error of the formation cycling baseline. Noting that the small SEI impedance rise indicates that some Li plating may be observed at 20% SOC, we revisit MST, but on a graphite electrode that was cycled 6 times to 20% SOC (yellow squares in Figure 6) instead of only 3 times. Although the average value of the inactive Li present on these electrodes is above the 0% SOC baseline (9 $\mu Ah/cm^2$ or 0.4% graphite capacity), it falls within the experimental error of the baseline values. Although additional trials could further elucidate this difference from baseline, the MST data here confirm that an onset of an increase in the graphite SEI resistance during fast charging is correlated with an onset of Li metal plating on the graphite surface, with a Li plating resolution of <0.6% graphite capacity. Given that it is also likely that not all of the additional inactive Li is from plated Li and that the 70% stripping efficiency could be a low estimate,[7] the sensitivity of SEI impedance rise to Li plating is likely even better than the 0.6% value reported here. However, because of the size of the electrodes used, lower plating percentages would be statistically the same as the baseline inactive Li, given the error in the titration technique. Titrations of larger format cells could be performed to more accurately determine the Li plating detection limit of the impedance analysis as a percentage of the total graphite capacity.

The impedance data were also compared to differential voltage relaxation analysis, or dOCV (Figure S6; Note S3). For the experimental conditions used here, dOCV does not indicate plating for any of the 20% or 30% cycles, only the 40% cycles. This is likely because the sensitivity of the impedance analysis to Li plating (<0.6% of graphite capacity) is higher than the reported sensitivity of dOCV analysis (1% of graphite capacity).[7]

Physical origin of impedance signal

The correlated onset of increased inactive Li measured via MST and the SEI impedance increase strongly suggests that these phenomena are related. However, that information alone is not sufficient to fully explain the physical origin of the impedance rise. Figure 7 helps visualize some possible explanations for the observed increase in SEI impedance signal. An increase in the SEI resistance could simply be due to Li metal breaking the SEI and forming additional species via reaction with the electrolyte (Figure 7A). It is also possible that the presence of metallic Li on the surface of graphite at one location leads to partial delamination and/or an increased transport resistance at the SEI/graphite interface (Figure 7B). It is also
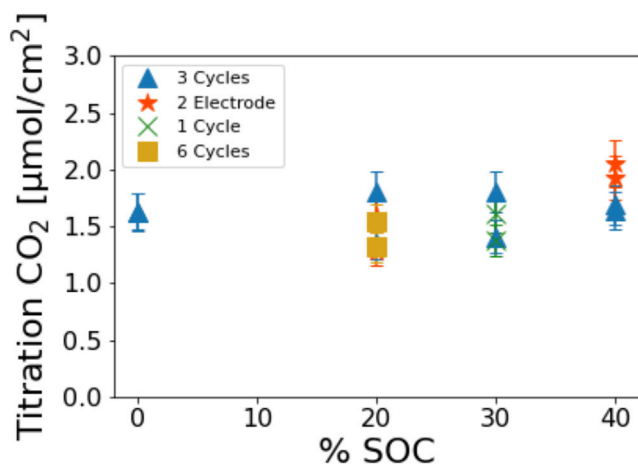
Figure 8. Quantifying carbonate-like species on graphite after fast charging
Measured CO_2 from MST of extracted and rinsed graphite electrodes post-cycling at a charge rate of 4C and deep discharge rate of C/2 to a graphite potential of 1.5 V versus Li/Li^+. The blue triangles are the results of electrodes cycled three times to the indicated SOC. The green crosses were cycled only once to the SOC. The red stars represent graphite electrodes cycled in a standard two-electrode full cell configuration. The yellow squares are the results of electrodes cycled six times to 20% SOC. The error bars are experimental errors determined to be 10% of the measured value.

possible that Li metal deposits protruding into the SEI simply create a longer transport length for a Li^+ to reach the graphite surface, effectively creating a more resistive SEI (Figure 7C).

MST also provides valuable information for measuring the formation of carbonate-like SEI species on the surface.[8] During the same MST experiments detailed in Figure 6, CO_2 evolution was also monitored. The reaction of SEI carbonates with acid to form CO_2 allows us to precisely measure how the amount of these species change with cycling. The results of this set of MST analyses are shown in Figure 8.

The amount of CO_2 titrated from the electrodes is approximately the same across all cycling conditions. This suggests that there is likely very little additional SEI formed during these XFC experiments. This is consistent with the results from McShane et al.,[8] who found that additional SEI only began forming after several XFC cycles and with substantially larger amounts of Li plated. This implies that the initial (and a small amount of) Li plating does not form above the initial graphite SEI nor does it break through the SEI. This is further supported if we look more closely at the low SOC impedance region in Figure 5A. We see there is no discernible difference in the SEI impedance from cycle to cycle. This further suggests no new SEI is formed, rather the observed impedance behavior is a reversible process, within the sensitivity limits of the impedance measurements. This supports some variation of the hypotheses presented in Figures 7B and 7C.

The high reversibility of the impedance increase, the relative magnitude of the rise in the R_{SEI} (~100% increase for 30% SOC cycling), and the high determined sensitivity of the technique support the hypothesis that a relatively small amount of Li is having a disproportionate effect on transport through the SEI. Namely, Li plating at one location on the SEI could increase strain laterally outward such that Li^+ transport to the graphite surface and/or transfer across the SEI/graphite interface is substantially hindered, as is illustrated in Figure 7B. Given that the OCV period would allow this strained region to relax and some metallic Li chemically inserts into the graphite

during the OCV, this hypothesis also reasonably explains the high level of reversibility. Additional experiments, such as cryo-transmission electron microscopy (TEM) imaging of Li metal deposits,[27] and possible simulations would need to be performed to more rigorously determine to what extent each of these phenomena explain the experimentally observed R_{SEI} increase during XFC. This behavior may also change with more cycles of 4C charging, i.e., aging of the cell may lead to less reversibility in the impedance increase from cycle to cycle.

Hahn et al.[22] suggest that plated Li deposits block Li^+ intercalation pathways into the graphite and decrease cell porosity, measured by an increase in the ionic pore resistance. With Li^+ transport lengths effectively increased, this in turn leads to an increase in both the charge transfer and the SEI resistances. For our system, Li plating is occurring at low SOC, before significant particle volume changes would occur, and assuming 70% stripping efficiency of the plated Li, the amounts of Li plated here are also quite small relative to the total pore volume (<0.1% of total electrode pore volume). Under different conditions, as with different electrolytes or for low temperature charging,[14,15,21] where plating morphology may change, the ionic resistance change in the pores may become an important factor. However, given this information, we do not believe pore blocking or particle volume increases are the direct cause of the observed behavior.

Applying *operando* impedance analysis to two-electrode full cells

Given the technical challenges posed by implementing reference electrodes in EV battery packs, it is highly preferred for any electrochemical Li plating detection method to perform well in standard two-electrode configurations. To evaluate the feasibility of applying our EIS techniques to two-electrode configurations, we must first examine the impedance response of the NMC532 cathode during XFC.

Figure 9A shows the high-frequency impedance response (100 kHz–1 kHz) of NMC532 during 4C XFC to 40%. This signal is related to cathode electrolyte interphase (CEI) resistance, as well as interparticle resistance in the composite electrode.[28] This process overlaps with the graphite SEI response, and as is clear when comparing to Figure 9B, it is larger than the graphite impedance. Additional details about the NMC532 impedance are discussed in Note S2 and Figure S5. However, it is also clear that the NMC532 impedance monotonically decreases with increasing SOC, and the graphite SEI response is fairly constant until it reaches some SOC where it begins increasing, i.e., the onset of plating around 15%–20% SOC. For a two-electrode system, one would be measuring the sum of these responses, simply referred to as the high-frequency "Hi-Freq" resistance in Figure 9. If no plating occurs, the graphite SEI response will remain constant and the full cell will simply reflect the monotonic decrease in the NMC high-frequency process, as is seen in Figure 9D. However, if plating does occur at some SOC, the graphite SEI resistance increase will offset the decreasing NMC impedance. And indeed, Figure 9C clearly shows this behavior starting around 15%–20% SOC. Despite charging at the same rate, Figure 9D does not indicate plating, whereas Figure 9C does. This is not unexpected, because the former cell configuration had twice the number of separators and thus twice the bulk resistance of the latter cell configuration. After the data collection shown in Figure 9, MST was performed on the extracted graphite electrode to confirm that Li plating did in fact occur (Figure 6; "2 electrode" measurement). Repeat experiments were performed wherein the electrodes were first cycled 3 times to 10% SOC and then 3 times to 20% SOC, as opposed to 3 cycles each to 10%, 20%, 30%, and 40% SOC, to get results closer to the onset predicted by impedance analysis. For these cells, the inactive Li on the graphite surface was indeed above the 0% SOC baseline: 13 $\mu Ah/cm^2$ or 0.6% graphite capacity. This is the same graphite capacity
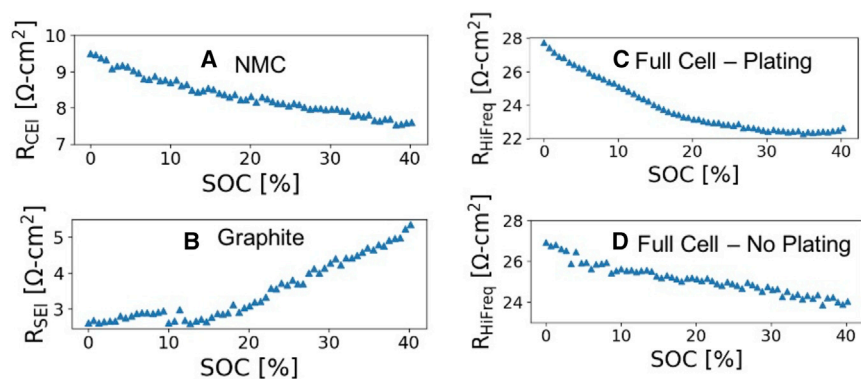
Figure 9. Comparing graphite and NMC532 high-frequency impedance during fast charging to full cell impedance

(A) The high-frequency resistance related to CEI and/or interparticle resistance on NMC532 during a 4C charge.

(B) This signal occurs in the same frequency regime ($\sim10^4$ Hz) as graphite SEI resistance during a 4C charge. The data for (A) and (B) were collected in a Gr/NMC532/AuLi three-electrode cell.

(C) The sum of these two impedance processes—"R_{HiFreq}"—is measured in an NMC532/Gr two-electrode cell during a 4C charge where plating occurs. This cell has the same number of separators as the three-electrode cell, two quartz fibers, and two Celgard 2500 separators.

(D) The same impedance frequency region as (C) but for a cell wherein impedance does not indicate Li plating. This cell has only one quartz fiber and one Celgard 2500 separator. The SOC for all of these is with respect to the capacity-limiting electrode, the NMC532.

See also Figure S5.

sensitivity, within rounding error, as we report for the 4C charging and plating experiments in the three-electrode cell configuration. This demonstrates that, even though the full cell impedance response is dominated by the NMC positive electrode's impedance, it is not necessary to resolve the graphite impedance to accurately detect Li plating during fast charging. Although additional work should be done to optimize this method for different cell types and electrode compositions, this clearly shows a proof of concept for *operando* impedance as a Li plating detection technique, with the onset of constant impedance as the marker for Li plating, in commercially relevant two-electrode, full-cell configurations.

This work demonstrates a potential *operando* electrochemical technique for the detection of Li plating. By taking impedance data while charging the battery, we can detect changes in the graphite SEI and charge transfer resistance. We have demonstrated that an increase in the SEI resistance appears to be particularly diagnostic for the onset of Li plating. This was confirmed using mass spectrometry titrations to quantify inactive Li after XFC and correlating it with the impedance response. This can be carried out at high rates (up to 6C and possibly higher) and is a non-destructive technique. Furthermore, it has a high Li plating detection resolution of <0.6% of graphite capacity. We have also demonstrated that this technique is applicable for commercially relevant two-electrode, full-cell configurations.

We have also outlined possible physical explanations for the observed impedance signals, supported by the titration results, as well as cycle-to-cycle impedance changes. Namely, we see a negligible change in the amount of CO_2 upon titration, no increase in the SEI baseline resistance with cycling, and a high reversibility in the impedance rise. Together, these results suggest the *operando* signal is possibly due to Li deposits significantly obstructing Li movement through the SEI and hindering transfer from the SEI to the graphite.

The primary limitation of this technique is that it requires one to charge the battery using AC impedance. Given the cost of impedance-capable potentiostat units, this likely prevents the widespread adoption of this technique for use in commercial charging stations for the time being. However, it could still prove invaluable for the battery research community.

Future work will entail further optimization and characterization of the limitations of this technique. This will namely involve determining the rate and cell age limits of the technique. There will be some maximum rate at which linear impedance can no longer be taken. There may also be some cell age at which other impedances dominate the signal and make the Li plating onset unresolvable, perhaps due to increased SEI resistance over the cycle life of the battery. We will also apply this technique to scaled-up systems, such as single- and multi-layer pouch cells to further demonstrate commercial applicability. We also intend to apply this technique to low-temperature battery operations, where Li plating is known to severely limit battery performance, even at much lower rates than XFC.[14,15,19,21,29]

EXPERIMENTAL PROCEDURES

Resource availability

Lead contact
Further information and requests for resources should be directed to and will be fulfilled by the lead contact, Bryan D. McCloskey (bmcclosk@berkeley.edu).

Materials availability
This study did not generate new unique reagents.

Data and code availability
The data that support the findings of this study are available from the lead contact upon reasonable request. This includes raw data from electrochemical tests and MSTs, as well as the post-processing Python scripts that were developed in house for DRT and dOCV analyses. The code for KK testing and other impedance analysis is publicly available on GitHub: https://github.com/kbknudsen/PyEIS.[30]

Electrodes for Li plating detection
Electrochemical tests for Li plating detection were performed using a graphite anode and a $LiNi_{0.5}Mn_{0.3}Co_{0.2}O_2$ (NMC532) cathode. The anode contained 91.8 wt % graphite (CGP-A12; Philips 66), 2 wt % of carbon black (C45; Timcal), 0.2 wt % oxalic acid, and 6 wt % poly(vinylidene difluoride) (PVDF) binder (KF-9300; Kureha). The cathode contained 90 wt % NMC532 (Toda) and 5 wt % of both carbon black (C45; Timcal) and PVDF (Solvay 5130). Slurries were coated on battery-grade copper and aluminum foils, respectively. The electrodes were calendared after drying, resulting in a thickness of 44 μm (37.4% porosity) for the anode and 71 μm (35.4% porosity) for the cathode; the areal active material loadings were 6.38 and 18.63 mg/cm^2, respectively. The electrodes were provided by the Argonne National Laboratory's Cell Analysis, Modeling, and Prototyping (CAMP) Facility.

Cell assembly
All three-electrode experiments were run in a custom-built cell, based on the design of Solchenbach et al.[31] (see also Figure S3 and supplemental experimental procedures). Each cell was assembled in an Ar glovebox with two quartz fiber separators (QMA; Whatman) and two polypropylene separators (Celgard 2500). The electrolyte for all tests is 1.2 M lithium hexafluorophosphate (LiPF$_6$) (Sigma-Aldrich) in a mixture of ethylene carbonate and ethyl methyl carbonate (EC:EMC) (BASF) in a 3:7 wt ratio.

A 12-mm graphite anode and 11-mm cathode are used for the working and counter electrodes. A 125-μm diameter Au wire insulated with PTFE (Goodfellow) is the reference electrode. 1 μAh of Li is alloyed with the tip of the Au wire to create a Li/Li$^+$ reference potential (~310 mV versus Li/Li$^+$) that we find is stable (± 5 mV) over the duration of our experiments. All two-electrode experiments were run in Swagelok-type cells using the same diameter electrodes and electrolyte as the three-electrode experiments. For all Li plating detection experiments, 3 formation cycles were performed with C/10 (10-h) charge and C/5 (5-h) discharge and 1.5 V to 10 mV versus Li/Li$^+$ cutoffs for the graphite electrode. Each fast-charging step is followed by a 30-min relaxation period to collect open-circuit voltage data for differential voltage relaxation analysis (see Figure S6 and Note S3).

Impedance measurements and DRT

All experimental data were gathered using a Bio-Logic VSP series potentiostat and at ambient temperature (21°C–24°C). The quality of impedance data was evaluated using KK analysis.[32,33] KK testing and DRT analysis of the data were performed using the PyEIS software, developed by Knudsen.[30] Additional information regarding the KK testing is located in Figure S1 and the supplemental experimental procedures.

For potentiostatic impedance measurements, the cells are charged to a certain SOC and allowed to rest for 30 min. After this rest period, an AC voltage perturbation of 5 mV is applied around the DC voltage measured at OCV. For these impedance measurements, the frequency range is 100 kHz to 100 mHz with 5 points per frequency decade and 2 measures per frequency.

For galvanostatic impedance measurements, a DC current is applied for a given C-rate with an overlying AC current with an amplitude equal to 15% of the DC current, except for the C/5 experiments where an AC amplitude equal to 50% of the DC current is required (see Supplemental experimental procedures for more details). The frequency range is 100 kHz to 50 Hz with 4 points collected per frequency decade and 2 measures per frequency. This leads to a per-scan time of approximately 6 s. Even for large DC currents (e.g., 6C), the short scan time allows for the linear and time invariant approximations to hold, as confirmed by KK analysis.

There are numerous methods for solving the DRT, but this study uses the DRT solution outlined by Ivers- Tiffée.[34] This solution, relevant analysis parameters, and the theoretical basis of the DRT are further outlined in Note S2 and Figure S4.

The peaks in the DRT are fitted with RQ circuit elements to extract the resistance and capacitance of the observed processes. This fitting necessarily ignores complexities of other circuit models, namely porous electrode effects that are better captured with transmission line models.[18,22] However, it is sufficient here to show the impedance effects of Li plating and fast charging. This is discussed further in Note S2 and Figure S4.

Mass spectrometry titrations

After a given fast-charging procedure, graphite electrodes are discharged to 1.5 V versus Li/Li$^+$ in 3 electrode cells, whereas two-electrode full cells are discharged to a full cell potential of 0 V. Graphite electrodes are then extracted inside a glovebox and rinsed three times for 1 min each time with 300 μL of DMC (BASF). The electrodes were then dried under active vacuum for 10 min.

All titrations were performed using the technique and equipment described by McShane et al.[8] In short, after the extraction and rinsing procedure, the electrodes

are placed inside an air-tight vessel that has capillaries. This vessel is then attached to a mass spectrometer via the capillaries. After obtaining baseline values of the desired mass fragments, sulfuric acid (2 mL, 3.5 M; BASF) is injected into the vessel. The acid reacts with the surface species, namely inactive Li species and carbonate-containing SEI species, to form hydrogen and carbon dioxide gases, respectively. These gases are fed to the mass spectrometer to obtain ion current counts of each species. These values are quantified using gas concentration calibration curves.

SUPPLEMENTAL INFORMATION

ACKNOWLEDGMENTS

AUTHOR CONTRIBUTIONS

DECLARATION OF INTERESTS

The authors declare no competing interests.

REFERENCES

1. Liu, Y., Zhu, Y., and Cui, Y. (2019). Challenges and opportunities towards fast-charging battery materials. Nat. Energy 4, 540–550.

2. Boyd, S. (2018). Batteries and electrification R&D overview. From a US Department of Energy (DOE) Vehicle Technologies Office (VTO) Annual Merit Review Meeting (AMR), June 2018. https://www.energy.gov/sites/prod/files/2018/06/f53/bat918_boyd_2018.pdf.

3. Gallagher, K.G., Dees, D.W., Jansen, A.N., Abraham, D.P., and Kang, S.-H. (2012). A volume averaged approach to the numerical modeling of phase-transition intercalation electrodes presented for Li_xC_6. J. Electrochem. Soc. 159, A2029–A2037.

4. Paul, P.P., McShane, E.J., Colclasure, A.M., Balsara, N., Brown, D.E., Cao, C., Chen, B.-R., Chinnam, P.R., Cui, Y., Dufek, E.J., et al. (2021). A review of existing and emerging methods for lithium detection and characterization in Li-ion

and Li-metal batteries. Adv. Energy Mater. *11*, 2100372.

5. Uhlmann, C., Illig, J., Ender, M., Schuster, R., and Ivers-Tiffée, E. (2015). In situ detection of lithium metal plating on graphite in experimental cells. J. Power Sources *279*, 428–438.

6. Burns, J.C., Stevens, D.A., and Dahn, J.R. (2015). In-situ detection of lithium plating using high precision coulometry. J. Electrochem. Soc. *162*, A959–A964.

7. Konz, Z.M., McShane, E.J., and McCloskey, B.D. (2020). Detecting the onset of lithium plating and monitoring fast charging performance with voltage relaxation. ACS Energy Lett. *5*, 1750–1757.

8. McShane, E.J., Colclasure, A.M., Brown, D.E., Konz, Z.M., Smith, K., and McCloskey, B.D. (2020). Quantification of inactive lithium and solid–electrolyte interphase species on graphite electrodes after fast charging. ACS Energy Lett. *5*, 2045–2051.

9. Waldmann, T., Hogg, B.-I., and Wohlfahrt-Mehrens, M. (2018). Li plating as unwanted side reaction in commercial Li-ion cells – a review. J. Power Sources *384*, 107–124.

10. Bugga, R.V., and Smart, M.C. (2010). Lithium plating behavior in lithium-ion cells. ECS Trans. *25*, 241–252.

11. Ringbeck, F., Rahe, C., Fuchs, G., and Sauer, D.U. (2020). Identification of lithium plating in lithium-ion batteries by electrical and optical methods. J. Electrochem. Soc. *167*, 090536.

12. Rodrigues, M.-T.F., Kalaga, K., Trask, S.E., Dees, D.W., Shkrob, I.A., and Abraham, D.P. (2019). Fast charging of Li-ion cells: part I. Using Li/Cu reference electrodes to probe individual electrode potentials. J. Electrochem. Soc. *166*, A996–A1003.

13. Schindler, S., Bauer, M., Petzl, M., and Danzer, M.A. (2016). Voltage relaxation and impedance spectroscopy as in-operando methods for the detection of lithium plating on graphitic anodes in commercial lithium-ion cells. J. Power Sources *304*, 170–180.

14. Chen, X., Li, L., Liu, M., Huang, T., and Yu, A. (2021). Detection of lithium plating in lithium-ion batteries by distribution of relaxation times. J. Power Sources *496*, 229867.

15. Katzer, F., and Danzer, M.A. (2021). Analysis and detection of lithium deposition after fast charging of lithium-ion batteries by investigating the impedance relaxation. J. Power Sources *503*, 230009.

16. Koleti, U.R., Dinh, T.Q., and Marco, J. (2020). A new on-line method for lithium plating detection in lithium-ion batteries. J. Power Sources *451*, 227798.

17. Schichlein, H., Müller, A.C., Voigts, M., Krügel, A., and Ivers-Tiffée, E. (2002). Deconvolution of electrochemical impedance spectra for the identification of electrode reaction mechanisms in solid oxide fuel cells. J. Appl. Electrochem. *32*, 875–882.

18. Illig, J., Ender, M., Weber, A., and Ivers-Tiffée, E. (2015). Modeling graphite anodes with serial and transmission line models. J. Power Sources *282*, 335–347.

19. Gantenbein, S., Weiss, M., and Ivers-Tiffée, E. (2018). Impedance based time-domain modeling of lithium-ion batteries: Part I. J. Power Sources *379*, 317–327.

20. Qu, H., Kafle, J., Harris, J., Zheng, D., Koshina, J., Boone, D., Drake, A.M., Abegglen, C.J., and Qu, D. (2019). Application of ac impedance as diagnostic tool – low temperature electrolyte for a Li-ion battery. Electrochim. Acta *322*, 134755.

21. Shafiei Sabet, P., Stahl, G., and Sauer, D.U. (2020). Non-invasive investigation of predominant processes in the impedance spectra of high energy lithium-ion batteries with nickel–cobalt–aluminum cathodes. J. Power Sources *472*, 228189.

22. Hahn, M., Schiela, A., Mößle, P., Katzer, F., and Danzer, M.A. (2020). Revealing inhomogeneities in electrode lithiation using a real-time discrete electro-chemical model. J. Power Sources *477*, 228672.

23. Schönleber, M., and Ivers-Tiffée, E. (2015). The *distribution function of differential capacity* as a new tool for analyzing the capacitive properties of Lithium-Ion batteries. Electrochem. Commun. *61*, 45–48.

24. Dahn, J.R. (1991). Phase diagram of $LixC6$. Phys. Rev. B Condens. Matter *44*, 9170–9177.

25. Orazem, M.E., and Tribollet, B. (2008). Electrochemical Impedance Spectroscopy, First Edition (John Wiley & Sons).

26. Diederichsen, K.M., McShane, E.J., and McCloskey, B.D. (2017). Promising routes to a high Li^+ transference number electrolyte for lithium ion batteries. ACS Energy Lett. *2*, 2563–2575.

27. Huang, W., Attia, P.M., Wang, H., Renfrew, S.E., Jin, N., Das, S., Zhang, Z., Boyle, D.T., Li, Y., Bazant, M.Z., et al. (2019). Evolution of the solid-electrolyte interphase on carbonaceous anodes visualized by atomic-resolution cryogenic electron microscopy. Nano Lett. *19*, 5140–5148.

28. Abarbanel, D.W., Nelson, K.J., and Dahn, J.R. (2016). Exploring impedance growth in high voltage NMC/graphite Li-ion cells using a transmission line model. J. Electrochem. Soc. *163*, A522–A529.

29. Waldmann, T., Wilka, M., Kasper, M., Fleischhammer, M., and Wohlfahrt-Mehrens, M. (2014). Temperature dependent ageing mechanisms in Lithium-ion batteries – a post-mortem study. J. Power Sources *262*, 129–135.

30. Knudsen, K. (2021). PyEIS: a Python-based electrochemical impedance spectroscopy simulator and analyzer. https://github.com/kbknudsen/PyEIS.

31. Solchenbach, S., Pritzl, D., Kong, E.J.Y., Landesfeind, J., and Gasteiger, H.A. (2016). A gold micro-reference electrode for impedance and potential measurements in lithium ion batteries. J. Electrochem. Soc. *163*, A2265–A2272.

32. Boukamp, B.A. (1993). Practical application of the Kramers-Kronig transformation on impedance measurements in solid state electrochemistry. Solid State Ion. *62*, 131–141.

33. Boukamp, B.A. (1995). A linear Kronig-Kramers transform test for immittance data validation. J. Electrochem. Soc. *142*, 1885.

34. Ivers-Tiffée, E., and Weber, A. (2017). Evaluation of electrochemical impedance spectra by the distribution of relaxation times. J. Ceram. Soc. Jpn. *125*, 193–201.